NANO LETTERS

LETTER

pubs.acs.org/NanoLett

Organic Multiferroic Tunnel Junctions with Ferroelectric Poly(vinylidene fluoride) Barriers

Juan M. López-Encarnación,[†,§] J. D. Burton,[‡] Evgeny Y. Tsymbal,[*,‡] and Julian P. Velev[*,†,‡]

[†]Department of Physics, Institute for Functional Nanomaterials, University of Puerto Rico, San Juan, Puerto Rico 00931

[‡]Department of Physics and Astronomy, Nebraska Center for Materials and Nanoscience, University of Nebraska, Lincoln, Nebraska 68588, United States

[§]Departamento de Física e Instituto de Física, Universidad Autónoma de Santo Domingo, Distrito Nacional, Dominican Republic 10105

S *Supporting Information*

ABSTRACT: Organic materials are promising for applications in spintronics due to their long spin-relaxation times in addition to their chemical flexibility and relatively low production costs. Most studies of organic materials for spintronics focus on nonpolar dielectrics or semiconductors, serving as passive elements in spin transport devices. Here, we demonstrate that employing organic ferroelectrics, such as poly(vinylidene fluoride) (PVDF), as barriers in magnetic tunnel junctions (MTJs) allows new functionality in controlling the tunneling spin polarization via the ferroelectric polarization of the barrier. Using first-principles methods based on density functional theory we investigate the spin-resolved conductance of Co/PVDF/Co and Co/PVDF/Fe/Co MTJs as model systems. We show that these tunnel junctions exhibit multiple resistance states associated with different magnetization configurations of the electrodes and ferroelectric polarization orientations of the barrier. Our results indicate that organic ferroelectrics may open a new and promising route in organic spintronics with implications for low-power electronics and nonvolatile data storage.

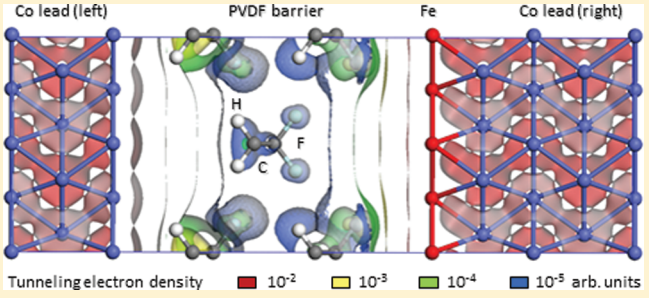

KEYWORDS: Electron tunneling, spintronics, organic ferroelectrics, organic tunnel junctions, multiferroic tunnel junctions

Organic materials have proven to be important for electronics by virtue of being cheap, environmentally friendly, flexible, easy to process, and offering virtually unlimited variations of functionality.[1,2] Recently it was demonstrated that organic materials are also very promising for spintronics, a branch of electronics that employs spin degrees of freedom in electronic devices.[3,4] This is due to a weak spin-orbit coupling that allows maintaining the spin information over large distances.[5,6] The first experiments by Dediu et al.[7] indicated a possibility to inject spins into an organic material, sexithiophene. Later, Xiong et al.[8] demonstrated a sizable spin-valve effect using an Alq_3 (tris-[8-hydroxyquinoline] aluminum) layer as a spacer between $La_{1-x}Sr_xMnO_3$ (LSMO) and Co electrodes. These results have stimulated significant research activity in studying spin transport across organic films.[9−14] Most experiments used a relatively thick (∼100 nm) organic layers in which the electron transport is via noncoherent hopping. Recently, there have been several successful attempts to produce thin organic barriers in which the transport is in the tunneling regime.[12−14] A particularly notable result is the observation of a large 300% tunneling magnetoresistance (TMR) in LSMO/Alq_3(2 nm)/Co MTJs by Barraud et al.,[14] where the possibility of chemical tuning of spin transport properties was demonstrated.

The above studies were focused on nonpolar dielectrics or semiconductors serving as passive elements in spin transport devices. In this work, we explore organic ferroelectrics as functional elements for spintronics applications. Organic ferroelectric polymers, such as poly(vinylidene fluoride) (PVDF) and related copolymers, form high quality ordered layers[15] and exhibit robust ferroelectricity down to monolayer thickness.[16] The electric polarization of PVDF is comparable to that of perovskite oxide ferroelectrics.[17] These properties make PVDF thin films promising for use as barriers in ferroelectric tunnel junctions (FTJs).[18] Because of their spontaneous polarization, which can be reversed by applied bias voltage, ferroelectric tunnel barriers allow switching of the tunneling conductance between two stable states. This phenomenon, known as tunneling electroresistance (TER), has been predicted theoretically.[19−21] Experimentally, the correlation between the ferroelectric polarization orientation and tunneling conductance was recently demonstrated by several groups on perovskite-oxide ferroelectric films.[22−24]

Using a ferroelectric thin film as barrier in a MTJ adds an additional level of functionality. In such a multiferroic tunnel

Received: October 18, 2010
Published: December 22, 2010

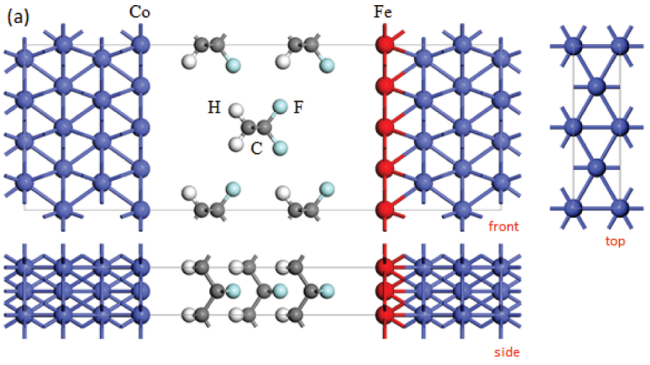

Figure 1. Atomic structure of (a) Co/PVDF/[Fe]/Co (0001) MFTJs with three monolayers of PVDF with its ferroelectric polarization pointing to the left.

junction (MFTJ), the TER and TMR effects coexist.[25] On the basis of first-principles calculations, simultaneous TER and TMR effects and multiple resistance states were demonstrated in $SrRuO_3/BaTiO_3/SrRuO_3$ MFTJs.[26] These calculations indicated, in particular, that the spin polarization of the tunneling conductance and hence TMR in MFTJs may be controlled by the ferroelectric polarization of the barrier. Recently, this behavior was observed experimentally in $Fe/BaTiO_3/LSMO$ MFTJs.[27]

The new functionality that allows electrically addressing spin degrees freedom may be brought to organic spintronics by employing organic ferroelectrics as tunnel barriers in MTJs. To explore the potential of such organic MFTJs, we consider Co/PVDF/Co and Co/PVDF/Fe/Co (0001) junctions, as shown schematically in Figure 1a. The ferroelectric polarization of PVDF $[-(CH_2-CF_2)_n-]$ is determined by the orientation of the CH_2-CF_2 monomer with the dipole moment pointing from F to H atoms. The reversal of ferroelectric polarization is associated with the rotation of the CH_2-CF_2 complex so that the H and F atoms are interchanged. Because of symmetric electrodes, the conductance in the zero-bias limit of the Co/PVDF/Co (0001) MFTJ is insensitive to the polarization orientation. To realize a four-state resistance device, we consider a Co/PVDF/Fe/Co (0001) MFTJ in which one monolayer of Fe is introduced at the right interface as shown in Figure 1a.

First, we analyze atomic and electronic structure of bulk PVDF. We use first-principles calculations based on density functional theory (DFT) implemented in a plane-wave pseudopotential method in the Quantum-Espresso (QE) package.[28] The Perdew-Burke-Ernzerhof (PBE) exchange-correlation functional with energy cutoff of 400 eV for the plane wave expansion and a $4 \times 12 \times 12$ Monkhorst-Pack grid for k-point sampling are used in the calculations. Further details are provided in the Supporting Information. We find that the body-centered orthorhombic structure of bulk PVDF is the most stable structure, in agreement with the previous studies.[29] The unit cell (a = 8.58, b = 5.12, c = 4.91 Å) contains two formula units along the polymer chain because of a small dihedral deflections (~7.2°) of the consecutive monomers (see Figure S1 in Supporting Information). The band gap of 5.8 eV is in good agreement with experiment (6.5 eV).[30] The spontaneous electric polarization of PVDF is 19.3 $\mu C/cm^2$ along the [001] direction, in agreement with previous calculations.[17]

In our structural model for PVDF-based MFTJs, we ignore for simplicity the dihedral deflections so that the unit cell contains only one VDF monomer along each of the polymer chains. This

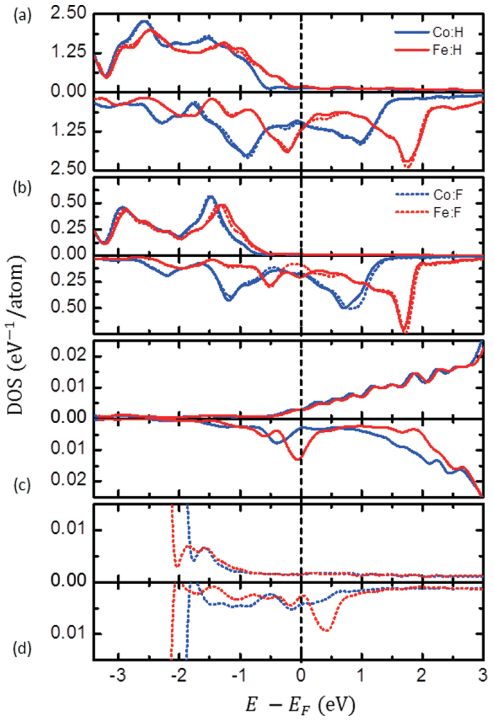

Figure 2. Spin-polarized local density of states (DOS) at the interfaces of Co/PVDF/Fe/Co MFTJ. (a) Total and (b) d_{z^2}-projected DOS on the Co and Fe interface atoms; (c) induced DOS on H and (d) F atoms adjacent to either Co or Fe. Majority-spin (top) and minority-spin (bottom panels) DOS are shown. Blue and red lines correspond to Co:X and Fe:X (X = H or F) interfaces, while solid and dashed lines correspond to X:H and X:F (X = Co or Fe).

PVDF unit cell has a good lattice match with hcp Co (a = 2.507, c = 4.069 Å) in its equivalent cubic cell. A Co 4×1 supercell (a = 8.685, b = 2.507 Å) matches within 2% with the PVDF cell where we choose the C chains to be atop of rows of Co. We find that PVDF is physisorbed on the metal surface and binding is obtained only if we take into account Van der Walls forces. To describe physisorption of PVDF on Co, we use the recently developed dispersion-corrected density functional theory (DFT-D), in which the Van der Walls interactions are included semiempirically (see Supporting Information).[31] The equilibrium interface distances were found to be 2.55 Å and 3.04 Å for the Co:H and Co:F interfaces respectively. Replacing Co with Fe at the interface produces small surface relaxation and small changes in the interface separations which we neglect in further calculations.

Figure 2 shows the calculated local density of states (DOS) in the Co/PVDF/Fe/Co MFTJs. By comparing deep core-like PVDF levels in the bulk and MFTJ, we find that the Fermi energy is located just about midgap of PVDF, that is, 2.8 eV above the valence band maximum and 3.0 eV below the conduction band minimum of the PVDF. The Co and Fe majority-spin 3d states (Figures 2a,b, top panels) are very similar and fully occupied, with only s-like density at and around the Fermi level. Correspondingly the induced majority-spin DOS at the Fermi level on the H and F interface atoms of the PVDF is nearly independent of the interface (Figures 2c,d, top panels). This is different from the minority-spin states, where the Fe-3d band is shifted up with respect to Co by about 0.8 eV (Figures 2a,b, bottom panels) due to the smaller number of valence electrons

dx.doi.org/10.1021/nl103650b |*Nano Lett.* 2011, 11, 599–603

and larger exchange splitting in Fe. The different electronic band structure of the minority-spin states in Fe and Co results in a very different induced minority-spin DOS on both the interface H and F atoms (Figures 2c,d, bottom panels).

This situation is reminiscent to that found by Barraud et al.[14] and discussed by Sanvito,[32] though in our junctions the features in the DOS are not due to the shift/broadening of intrinsic atomic levels on the organic molecules. Instead the peaks seen in Figures 2c,d (bottom panels) near the Fermi energy are metal-induced gap states (MIGS) that originate from minority-spin states of the Co and Fe surface and contribute to the tunneling. The energy of these states is quite sensitive to the atomic species of the neighboring PVDF termination and thus to the orientation of the ferroelectric polarization.

Examining the d_{z^2} orbital projection on the Fe atoms reveals a substantial change in the DOS at and around the Fermi level upon ferroelectric switching (compare solid and dashed red curves in Figure 2b). The sensitivity of the d_{z^2} states comes from the fact that this orbital has a lobe of electronic density oriented perpendicular to the Fe surface. When the ferroelectric polarization is to the right, and therefore the positive H atoms are closest to the Fe surface, it is energetically favorable for these states to be occupied, that is, lower in energy, because this moves negative charge toward the positive PVDF surface. When the negatively charged F atoms are closer, however, it is unfavorable for them to be occupied, that is, the Fe d_{z^2} states move up in energy. The Co d_{z^2} orbitals at the other interface are also affected by the ferroelectric switching. However, since the Co states lie deeper in energy, DOS does not appreciably change the occupation near the Fermi level. States deriving from the d_{z^2} (and s) orbitals, which have long tails along the z direction, contribute significantly to the tunneling transport as compared to states deriving from other orbitals. The enhancement/suppression of the density of these states at the Fermi level upon polarization switching alters MIGS (e.g., peak in the H DOS and dip in the F DOS at the Fe interface, Figures 2c,d). These are entirely consistent with the results of our transport calculations as discussed below.

The conductance is calculated using a general scattering formalism[33,34] implemented in the QE package.[28] The structure of Figure 1 is considered as the scattering region, ideally attached on both sides to semi-infinite hcp Co leads. The transmission and reflection matrices are then obtained by matching the wave functions in the scattering region to appropriate linear combinations of the Bloch states in the left and right leads. The conductance calculations are performed at zero bias using a uniform 30×100 k-point mesh in the two-dimensional Brillouin zone. Table 1 summarizes results for the conductance of the MFTJs computed for parallel (P) and antiparallel (AP) magnetization orientation of the electrodes. We define the TMR ratio as TMR = $(G_P - G_{AP})/(G_P + G_{AP})$, where $G_P = G_{\uparrow\uparrow} + G_{\downarrow\downarrow}$ is the conductance for the P configuration, $G_{AP} = G_{\uparrow\downarrow} + G_{\downarrow\uparrow}$ the conductance for the AP configuration, and vertical arrows indicate the spin direction. The conductance for AP configuration is calculated by doubling the unit cell in the current direction and setting the magnetization in the second Co slab opposite to the first. The TER ratio is given by TER = $(G_{\leftarrow} - G_{\rightarrow})/(G_{\leftarrow} + G_{\rightarrow})$, where $G_{\leftarrow}$ is the conductance for the PVDF polarization pointing to the left, $G_{\rightarrow}$ the conductance for the PVDF polarization pointing to the right, and horizontal arrows indicate the polarization direction.

As seen from Table 1, for the Co/PVDF/Co MFTJ we obtain a minority-spin dominated conductance and inverse TMR. TMR

Table 1. Conductance Per Unit Cell Area, TMR and TER for Co/PVDF/[Fe]/Co (0001) MFTJs[a]

	G (10^{-5} e^2/h)			TMR (%)
	↑↑	↓↓	↑↓ + ↓↑	
	Co/PVDF/Co			
←(→)	1.04	2.36	4.71	−16.3
	Co/PVDF/Fe/Co			
←	1.57	0.60	1.53	17.3
→	1.00	33.62	16.71	34.9
TER (%)		−88.2	−83.2	

[a] Majority- and minority-spin conductance for parallel magnetization of the electrodes (↑↑ and ↓↓, respectively) and the total conductance for the antiparallel magnetization (↑↓+↓↑) are shown for the PVDF polarization oriented left (←) and right (→).

can be analyzed in terms of the interface transmission functions (ITFs).[35] Qualitatively the TMR can be expressed as TMR = $P_{Co:H}P_{Co:F}$, where the interface spin polarizations $P_{Co:H}$ and $P_{Co:F}$ are determined by the average spin dependent ITFs $T^{\uparrow}$ and $T^{\downarrow}$, that is, $P = (T^{\uparrow} - T^{\downarrow})/(T^{\uparrow} + T^{\downarrow})$ (see Supporting Information). Since the ITFs are proportional to the induced DOS in the barrier,[35] we can read off from Figures 2c,d that $T^{\uparrow}_{Co:H} > T^{\downarrow}_{Co:H}$ and $T^{\uparrow}_{Co:F} < T^{\downarrow}_{Co:F}$, and therefore, $P_{Co:H} > 0$ and $P_{Co:F} < 0$ which explains the inverse TMR.

Figure 3a shows the $\mathbf{k}_{||}$-resolved transmission calculated within the two-dimensional Brillouin zone for the Co/PVDF/Co MFTJ. It is seen that both the majority- and minority-spin transmission have ellipse-shaped distributions centered at the $\bar{\Gamma}$ point ($\mathbf{k}_{||} = 0$), which are reminiscent to the transmission found for the face-centered cubic Co(111) surface.[35] The minority-spin transmission is larger than the majority-spin transmission due to a large number of electronic states at the Fermi energy (conductance channels) available for the minority spins in bulk Co. As stated earlier, the TER is zero for this junction.

This is contrary to the Co/PVDF/Fe/Co MFTJ that exhibits a very large TER effect with the conductance for polarization oriented right being by an order of magnitude higher than the conductance for polarization oriented left. As seen from Table 1, the majority-spin conductance in the parallel configuration changes insignificantly when the ferroelectric polarization is switched and remains nearly the same as for the Co/PVDF/Co MFTJ. On the other hand, the minority-spin conductance changes dramatically with polarization reversal. The whole spin transport regime is altered from minority- to majority-spin dominated when the polarization switches from left to right. Figure 3b,c shows the $\mathbf{k}_{||}$-resolved transmission for the Co/PVDF/Fe/Co MFTJ. It is seen that the transmission has the same features as for in the Co/PVDF/Co MFTJ except that the minority-spin intensity is enhanced (reduced) when the ferroelectric polarization is pointing to the right (left), that is, for (Co:F, Fe:H) and (Co:H, Fe:F) interfaces, respectively. This behavior is consistent with a larger induced DOS at the Fermi energy by the Fe (Co) electrode on the interface H (F) atom than the other way around (Figure 2c,d).

These results are consistent with the ITF-based model. We observe that $T^{\downarrow}_{Co:H} < T^{\downarrow}_{Fe:H}$ and $T^{\downarrow}_{Co:F} > T^{\downarrow}_{Fe:F}$. This can be seen, on one hand, from the DOS on the H and F atoms at the Fermi energy (Figures 2c,d). On the other hand, this follows from the

dx.doi.org/10.1021/nl103650b |Nano Lett. 2011, 11, 599–603

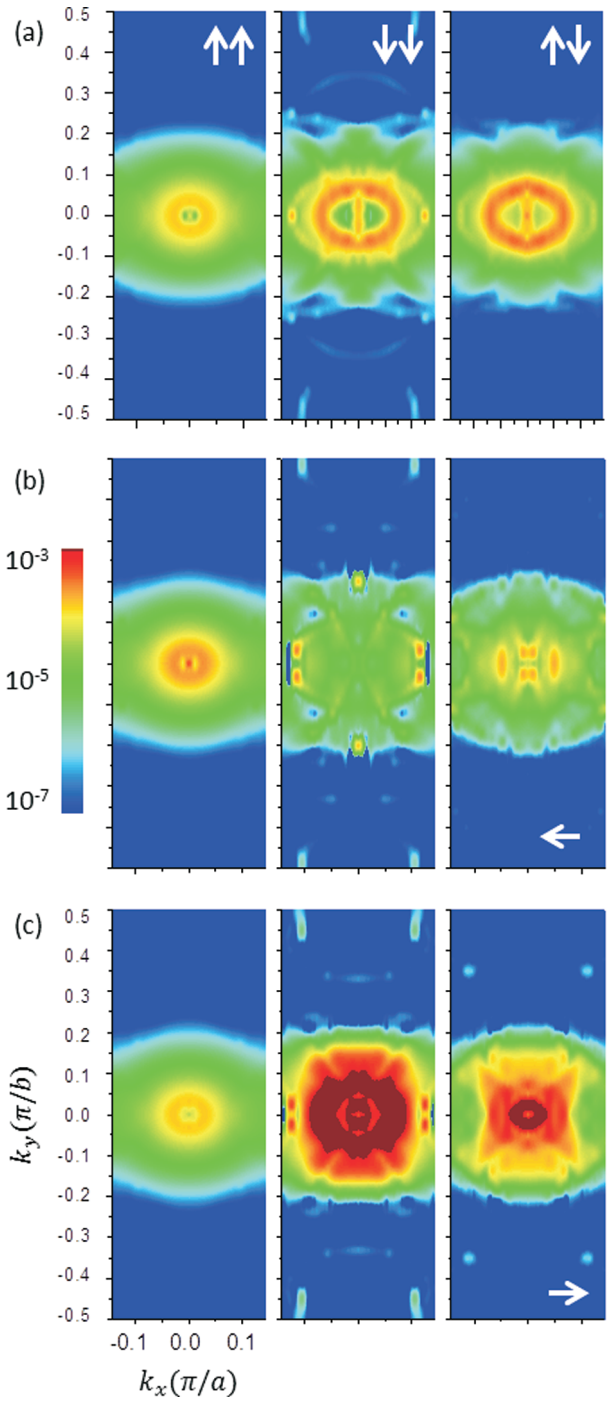

Figure 3. $\mathbf{k}_{||}$-resolved spin-dependent transmission within the two-dimensional Brillouin zone for Co/PVDF/Co MFTJ (a) and for Co/PVDF/Fe/Co MFTJ for the PVDF polarization pointing to the left (b) and to the right (c). The transmission is shown for majority- (left) and minority- (middle panels) spin electrons for the parallel magnetization alignment of the electrodes and average of the two spin channels for the antiparallel magnetization (right panels).

$\mathbf{k}_{||}$-resolved transmission (Figures 3b,c) where for each $\mathbf{k}_{||}$ in the area dominating the transmission these inequalities hold, which justifies replacing the $\mathbf{k}_{||}$-dependent ITFs with their averages. Then, since the conductance is proportional to the average ITFs at both interfaces, for the Co/PVDF/Co junction we have $G^{\downarrow\downarrow} \sim T^{\downarrow}_{\mathrm{Co:H}} T^{\downarrow}_{\mathrm{Co:F}}$. For the Co/PVDF/Fe/Co, we obtain $G^{\downarrow\downarrow}_{\leftarrow} \sim T^{\downarrow}_{\mathrm{Co:H}} T^{\downarrow}_{\mathrm{Fe:F}}$ for polarization to the left and $G^{\downarrow\downarrow}_{\rightarrow} \sim T^{\downarrow}_{\mathrm{Co:F}} T^{\downarrow}_{\mathrm{Fe:H}}$ for polarization to the right. From there we can conclude that $G^{\downarrow\downarrow}_{\leftarrow} < G^{\downarrow\downarrow} < G^{\downarrow\downarrow}_{\rightarrow}$ holds for the conductance.

The key feature of the organic MFTJs is the possibility to control the transport spin polarization and TMR by ferroelectric polarization orientation. We already found that interface spin polarization for the Co interface is reversed with polarization switching $P_{\mathrm{Co:H}} > 0$ and $P_{\mathrm{Co:F}} < 0$. Similar behavior is observed for the Fe interface, where $T^{\uparrow}_{\mathrm{Fe:H}} < T^{\downarrow}_{\mathrm{Fe:H}}$ and $T^{\uparrow}_{\mathrm{Fe:F}} > T^{\downarrow}_{\mathrm{Fe:F}}$ and thus the interface spin polarization changes sign from $P_{\mathrm{Fe:H}} < 0$ to $P_{\mathrm{Fe:F}} > 0$ upon polarization switching. Moreover, the spin polarizations of the Co and Fe interfaces are opposite. Although the predicted TMR is positive for both orientations of polarization, $\mathrm{TMR}_{\leftarrow} = P_{\mathrm{Co:H}} P_{\mathrm{Fe:F}} > 0$ and $\mathrm{TMR}_{\rightarrow} = P_{\mathrm{Co:F}} P_{\mathrm{Fe:H}} > 0$, it is very different in magnitude because the conductance is dominated by different spin channels.

Overall, employing ferroelectric organic thin films as tunnel barriers in magnetic tunnel junctions brings new functionalities to organic electronics and spintronics. The nature of ferroelectric switching in organic polymers involves a physical change of the atomic species at the interface that allows controlling the electron and spin transport. The predicted giant TER, sizable TMR, and the control of the interface spin polarization and TMR by ferroelectric polarization switching involve interesting physics and are promising for applications. We therefore hope that our theoretical predictions will stimulate experimental studies of magnetic tunnel junctions with organic ferroelectric barriers.

■ ASSOCIATED CONTENT

Supporting Information. Poly(vinylidene fluoride) structure and electronic properties, interface separation between Co and PVDF, model for the conductance, additional figures, additional table, and additional references. This material is available free of charge via the Internet at http://pubs.acs.org.

■ AUTHOR INFORMATION

Corresponding Author

*E-mail: (E.Y.T.) tsymbal@unl.edu; (J.P.V.) jvelev@gmail.com.

■ ACKNOWLEDGMENT

This work was supported by the National Science Foundation (NSF) through Institute of Functional Nanomaterials (NSF grant 0701525) at University of Puerto Rico (UPR), Materials Research Science and Engineering Center (NSF grant 0820521) at University of Nebraska-Lincoln (UNL), and the Experimental Program to Stimulate Competitive Research (NSF grants EPS-1010674 and EPS-1010094). Computations were performed at the UPR High Performance Computing facility and the UNL Holland Computing Center. J.M.L.-E. is grateful to Daniel Forrer by his help with the DFT-D code.

■ REFERENCES

(1) Dediu, V. A.; Hueso, L. E.; Bergenti, I.; Taliani, C. *Nat. Mater.* **2009**, *8*, 707–716.

(2) Szulczewski, G.; Sanvito, S.; Coey, J. M. D. *Nat. Mater.* **2009**, *8*, 693–695.

(3) Chappert, C.; Fert, A.; Van Dau, F. N. *Nat. Mater.* **2007**, *6*, 813–823.

(4) Velev, J. P.; Dowben, P. A.; Tsymbal, E. Y.; Jenkins, S. J.; Caruso, A. N. *Surf. Sci. Rep.* **2008**, *63*, 400–425.

(5) Drew, A. J.; Hoppler, J.; Schulz, L.; Pratt, F. L.; Desai, P.; Shakya, P.; Kreouzis, T.; Gillin, W. P.; Suter, A.; Morley, N. A.; Malik, V. K.; Dubroka, A.; Kim, K. W.; Bouyanfif, H.; Bourqui, F.; Bernhard, C.; Scheuermann, R.; Nieuwenhuys, G. J.; Prokscha, T.; Morenzoni, E. *Nat. Mater.* **2009,** *8*, 109–114.
(6) Cinchetti, M.; Heimer, K.; Wüstenberg, J.-P.; Andreyev, O.; Bauer, M.; Lach, S.; Ziegler, C.; Gao, Y.; Aeschlimann, M. *Nat. Mater.* **2009,** *8*, 115–119.
(7) Dediu, V.; Murgia, M.; Matacotta, F. C.; Taliani, C.; Barbanera, S. *Solid State Commun.* **2002,** *122*, 181–184.
(8) Xiong, Z. H.; Wu, D.; Vardeny, Z. V.; Shi, J. *Nature* **2004,** *427*, 821–824.
(9) Wang, F. J.; Yang, C. G.; Vardeny, Z. V.; Li, X. *Phys. Rev. B* **2007,** *75*, No. 245324.
(10) Dediu, V. A.; Hueso, L. E.; Bergenti, I.; Riminucci, A.; Borgatti, F.; Graziosi, P.; Newby, C.; Casoli, F.; De Jong, M. P.; Taliani, C.; Zhan, Y. *Phys. Rev. B* **2008,** *78*, No. 115203.
(11) Sun, D.; Yin, L.; Sun, C.; Guo, H.; Gai, Z.; Zhang, X.-G.; Ward, T. Z.; Cheng, Z.; Shen, J. *Phys. Rev. Lett.* **2010,** *104*, No. 236602.
(12) Santos, T. S.; Lee, J. S.; Migdal, P.; Lekshmi, I. C.; Satpati, B.; Moodera, J. S. *Phys. Rev. Lett.* **2007,** *98*, No. 016601.
(13) Yoo, J. W.; Chen, C. Y.; Jang, H. W.; Bark, C. W.; Prigodin, V. N.; Eom, C. B.; Epstein, A. J. *Nat. Mater.* **2010,** *9*, 638–642.
(14) Barraud, C.; Seneor, P.; Mattana, R.; Fusil, S.; Bouzehouane, K.; Deranlot, C.; Graziosi, P.; Hueso, L.; Bergenti, I.; Dediu, V. A.; Petroff, F.; Fert, A. *Nat. Phys.* **2010,** *6*, 615–642.
(15) Lovinger, A. J. *Science* **1983,** *220*, 1115–1121.
(16) Bune, A. V.; Fridkin, V. M.; Ducharme, S.; Blinov, L. M.; Palto, S. P.; Sorokin, A.; Yudin, S. G.; Zlatkin, A. *Nature* **1998,** *391*, 874–877.
(17) Nakhmanson, S. M.; Nardelli, M. B.; Bernholc, J. *Phys. Rev. B* **2005,** *72*, No. 115210.
(18) Tsymbal, E. Y.; Kohlstedt, H. *Science* **2006,** *313*, 181–183.
(19) Zhuravlev, M. Y.; Sabirianov, R. F.; Jaswal, S. S.; Tsymbal, E. Y. *Phys. Rev. Lett.* **2005,** *94*, No. 246802.
(20) Kohlstedt, H.; Pertsev, N. A.; Rodriguez Contreras, J.; Waser, R. *Phys. Rev. B* **2005,** *72*, No. 125341.
(21) Velev, J. P.; Duan, C.-G.; Belashchenko, K. D.; Jaswal, S. S.; Tsymbal, E. Y. *Phys. Rev. Lett.* **2007,** *98*, No. 137201.
(22) Garcia, V.; Fusil, S.; Bouzehouane, K.; Enouz-Vedrenne, S.; Mathur, N. D.; Barthélémy, A.; Bibes, M. *Nature* **2009,** *460*, 81–84.
(23) Maksymovych, P.; Jesse, S.; Yu, P.; Ramesh, R.; Baddorf, A. P.; Kalinin, S. V. *Science* **2009,** *324*, 1421–1425.
(24) Gruverman, A.; Wu, D.; Lu, H.; Wang, Y.; Jang, H. W.; Folkman, C. M.; Zhuravlev, M. Y.; Felker, D.; Rzchowski, M.; Eom, C.-B.; Tsymbal, E. Y. *Nano Lett.* **2009,** *9*, 3539–3543.
(25) Zhuravlev, M. Y.; Jaswal, S. S.; Tsymbal, E. Y.; Sabirianov, R. F. *Appl. Phys. Lett.* **2005,** *87*, No. 222114.
(26) Velev, J. P.; Duan, C.-G.; Burton, J. D.; Smogunov, A.; Niranjan, M. K.; Tosatti, E.; Jaswal, S. S.; Tsymbal, E. Y. *Nano Lett.* **2009,** *9*, 427–432.
(27) Garcia, V.; Bibes, M.; Bocher, L.; Valencia, S.; Kronast, F.; Crassous, A.; Moya, X.; Vedrenne, S. E.; Gloter, A.; Imhoff, D.; Deranlot, C.; Mathur, N. D.; Fusil, S.; Bouzehouane, K.; Barthélémy, A. *Science* **2010,** *327*, 1106–1110.
(28) Giannozzi, P.; Baroni, S.; Bonini, N.; Calandra, M.; Car, R.; Cavazzoni, C.; Ceresoli, D.; Chiarotti, G. L.; Cococcioni, M.; Dabo, I.; Corso, A. D.; Gironcoli, S. D.; Fabris, S.; Fratesi, G.; Gebauer, R.; Gerstmann, U.; Gougoussis, C.; Kokalj, A.; Lazzeri, M.; Martin-Samos, L.; Marzari, N.; Mauri, F.; Mazzarello, R.; Paolini, S.; Pasquarello, A.; Paulatto, L.; Sbraccia, C.; Scandolo, S.; Sclauzero, G.; Seitsonen, A. P.; Smogunov, A.; Umari, P.; Wentzcovitch, R. M. *J. Phys.: Condens. Matter* **2009,** *21*, No. 395502 URL: http://www.quantum-espresso.org.
(29) Carbeck, J. D.; Lacks, D. J.; Rutledge, G. C. *J. Chem. Phys.* **1995,** *103*, 10347–10355.
(30) Choi, J.; Dowben, P. A.; Pebley, S.; Bune, A. V.; Ducharme, S.; Fridkin, V. M.; Palto, S. P.; Petukhova, N. *Phys. Rev. Lett.* **1998,** *80*, 1328–1331.
(31) Barone, V.; Casarin, M.; Forrer, D.; Pavone, M.; Sambi, M.; Vittadini, A. *J. Comput. Chem.* **2009,** *30*, 934–939.
(32) Sanvito, S. *Nat. Phys.* **2010,** *6*, 562–564.
(33) Choi, H. J.; Ihm, J. *Phys. Rev. B* **1999,** *59*, 2267–2275.
(34) Smogunov, A.; Dal Corso, A.; Tosatti, E. *Phys. Rev. B* **2004,** *70*, 045417.
(35) Belashchenko, K. D.; Tsymbal, E. Y.; van Schilfgaarde, M.; Stewart, D.; Oleinik, I. I.; Jaswal, S. S. *Phys. Rev. B* **2004,** *69*, No. 174408.